URSI GASS 2020, Rome, Italy, 29 August - 5 September 2020

Laser-machined substrate technology (LMST) for Q-band applications

A. Fontana[(1)], *Student Member, IEEE*, A. Perigaud [(1)], P. Richard[(2)], D. Carsenat[(2)], R. Elmostadi[(2)] and N. Delhote*[(1)]
(1) Univ. Limoges, XLIM, UMR 7252, F-87000 Limoges, France, www.xlim.fr
(2) Thales SIX GTS, F-19100 Brive-la-Gaillarde, France

Abstract

A three-steps laser micro-machined manufacturing technology (LMST) based in low-loss Alumina substrates is introduced and studied. As a consequence of this analysis, fabrication constraints are identified and design rules introduced in order to assist the conception of millimeter-wave passive devices for Q-band applications. Quality factor around 690 is measured at 42 GHz in resonators fabricated with this technology. Moreover, diverse devices are designed with the design rules proposed. Manufactured devices show good repeatability and balance between performance and size.

1 Introduction

The important growth in data transfer and wireless communications during the last decade has led to an increase on the demand of broadband channels. New incoming communication technologies such as the fifth generation (5G) require more capacity and data performance than previous technologies [1]. The need to fulfill those requirements encouraged researches to push conventional communication systems from sub-6 GHz bands to higher frequencies bands such as Q-band, V-band and E-band, used so far for military and radar applications. Millimeter-wave (mm-Wave) broadcasting emerges as a promising solution to provide higher bandwidth, data rate and spectrum efficiency for point-to-point communications, inter-satellite links, semi-autonomous 5G networks, vehicular communication, health care applications, among others. Several new bands (24.25 – 27.5, 31.8 – 33.4, 37 – 40.5, 40.5 – 42.5, 42.5 - 43.5, 45.5 - 47, 47 - 47.2 and 47.2 - 50.2 GHz) for 5G worldwide deployments have been treated recently by WRC-19 [2].
Many technological approaches [3] with different balances between manufacturing dispersion, cost, number of stages, size, electromagnetic (EM) performances and temperature stability have been proposed so far for mm-Wave applications. For example, in organic-substrate SIW, temperature instability and high loss tangent limit the quality factor (Q), a problem that was successfully solved by air filled SIW technology. In multistep processes such as LTCC, high 3-D integration can be obtained at expense of demanding alignment constraints and elevated prototyping costs. Technologies such as stacked micro-machined silicon wafers and miniature coaxial resonators must be fabricated in very well monitored environments (clean rooms). An alternative technology based on laser micro-machined process and 3-D plating was proposed in [4]. In this work, a process analysis is performed in order to assess LMST limitations. Useful design rules and constraints for Alumina based substrates are identified to provide a reliable method for Q-band applications. Finally, SIW components designed at 42 GHz for mm-Wave frequencies are introduced and discussed.

2 Fabrication flow

Fig. 1 shows a three-steps laser machining fabrication flow for passive devices manufacturing. It is interesting to note that this fabrication flow is independent of the substrate. The first step consists in the substrate machining by means of a laser. The needed laser accuracy depends mostly on the frequency range of the device. For Q-band applications, accuracy should be around tens of micrometers to avoid critical deviations. A 25 µm spot YAG laser with 10 um manufacturing accuracy was employed to accomplish specifications between 39 and 45 GHz. In addition, improvements in the quality factor can be achieved with proper metallization and loss tangent reduction [5]. Ceramic materials are an interesting option for these applications thanks to their good electromagnetic properties (low losses, high ε_r and thermal stability). Hence, very low-loss Alumina substrates [6] ($\varepsilon_r = 9.8 \pm 0.4$ and $tan\delta = 5.10^{-4}$ at 42 GHz) were used for the study. Quality factor can also be improved with thicker substrates, nevertheless, maximum thickness is li-

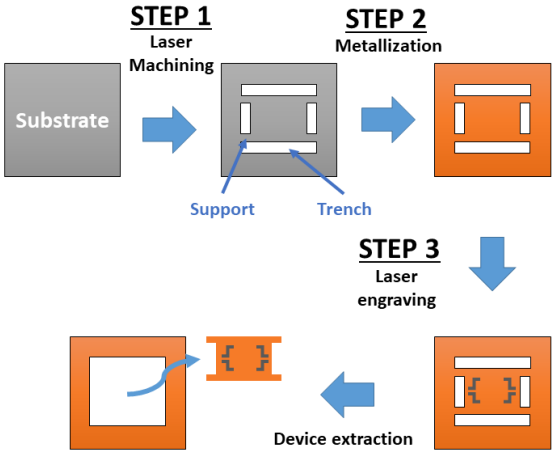

Figure 1. Laser micro-machined fabrication flow.

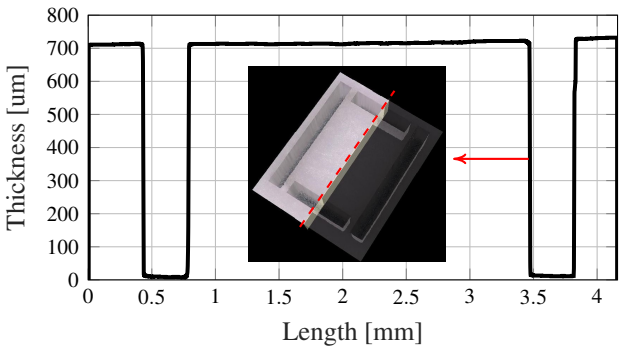

Figure 2. Resonator thickness measured with a digital microscope. Maximum thickness of 732 µm is due to 55 µm separation between the microscope stage and the substrate.

mited to roughly 0.7 mm to maintain the laser well focused during the machining. Vertical walls in a 0.66 mm thickness substrate were characterized to determine their quality and size dispersion. Measurements acquired with a digital microscope (fig. 2) show slopes with typical differences between 4 and 5 µm. Therefore, vertical walls dispersion cannot be neglected and must be taken into account during the design. Final manufacturing deviation (15 µm) results in much lower dispersion than typical PCB or LTCC processes and is in a good compromise between Q improvement and fabrication accuracy. After laser machining (step 1), metal coating with Jet Metal© or electroless copper is performed on the structure (step 2). To obtain an attenuation higher than seven times the penetration depth at 42 GHz, a 3 µm (silver)/5 µm (copper) metal layer is deposited depending on the employed process. A final protective gold layer (0.2 µm) is applied with electrolysis in the case of electroless copper. In the end, laser etching (step 3) followed by the device extraction is carried on to engrave input/output accesses, coplanar lines or SMD pads on the top/bottom metal surface. To avoid frictions that could hinder the extraction between the device and the substrate walls, trenches should be added during the first step to facilitate the removal (fig. 1). Moreover, trenches could be useful to improve the particle flux during the metal coating process. The device remains attached to the substrate through supports as shown in fig. 1. To be able to remove the excess material, the minimum size for trenches in Alumina substrates is 160 µm while the minimum width to avoid cracks on the supports is 200 µm. A theoretical Q around 700 is expected for devices fabricated with this process and metallized with Jet Metal silver coating. Even when the thickness restriction confines the design to 2.5-D devices, a diverse amount of SIW-like components can be developed.

3 Laser-machined devices

A set of Alumina-based passive devices were designed and manufactured at 40.5 - 43.5 GHz with the fabrication flow explained in Section 2. Instead of typical SIW with vias, the devices are directly trimmed in the substrate allowing to use them as wire bonded/flip-chipped discrete devices or as substrates to create more complex subsystems. Coplanar accesses were optimized for direct probing measurements.

Table 1. Measured dispersion in manufactured resonators.

	Resonator 1	Resonator 2
$Width(W)$	2.102 mm	2.090 mm
$Length(L)$	2.687 mm	2.676 mm
$\|\Delta W\|$	20 µm	30 µm
$\|\Delta L\|$	13 µm	24 µm
$\|\Delta fo(TE_{102})\|_{@42GHz}$	296 MHz	331 MHz
$\|\Delta fo(TE_{101})\|_{@28.72GHz}$	223 MHz	249 MHz
$\varepsilon_{r_{@42GHz}}$	10.08	10.16
$Q_{@42GHz}$	673	689

3.1 Rectangular cavity resonator

Resonators are key basic blocks for filter design, and permittivity and loss estimation. Rectangular resonators operating in the fundamental mode TE_{101} are smaller than higher order modes and ideal for compact single-mode filters. However, they have lower Q and are more sensitive to fabrication dispersion. Considering a reduction of 30 µm on the length and width of the resonator, a frequency shift of $\Delta f_{TE_{101}} = 808\ MHz$ is expected for a 1.6 mm x 1.6 mm TE101 resonator at 42 GHz. On the other hand, a 2.12 mm x 2.70 mm TE_{102} resonator has a frequency shift of $\Delta f_{TE_{102}} = 511\ MHz$ for the same conditions. Furthermore, an increment of 19.5% in Q can be addressed when using the mode TE_{102} at the same frequency in expense of 46.8% area increasing. Permitivitty discrepancies have the same influence on the frequency shift for both modes (e.g., a variation of $|\varepsilon_r = 0.2|$ produces $|\Delta f_{TE_{101}}| = |\Delta f_{TE_{102}}| = 436\ MHz$). Therefore, TE_{102} resonators are less affected by fabrication dispersion and more suitable for electrical characterization. To characterize the EM properties of the Alumina substrate, a TE_{102} rectangular cavity resonator was designed at 42 GHz. Table 1 summarizes the measured size, frequency shifting, ε_r and Q for two manufactured TE_{102} resonators with the fundamental mode located at 28.72 GHz. Size variations up to 30 µm are observed confirming the predicted process dispersion and maximum $|\Delta fo(TE_{102})| = 331\ MHz$ is obtained (table 1). Quality factors of 673 and 689 were measured from these manufactured resonators and permitivitty around 10.1 was calculated.

3.2 Rectangular waveguide

Waveguides are other useful passive elements in mm-Wave systems for EM wave transmission. A rectangular waveguide proposed for Q-band applications is shown in fig. 3. Cutoff frequency for the fundamental TE_{10} mode is located at 34.5 GHz while the transmission for the second mode TE_{20} starts at 66 GHz. The total device dimension is 1.45 mm x 6.00 mm. Four supports of 200 µm width and

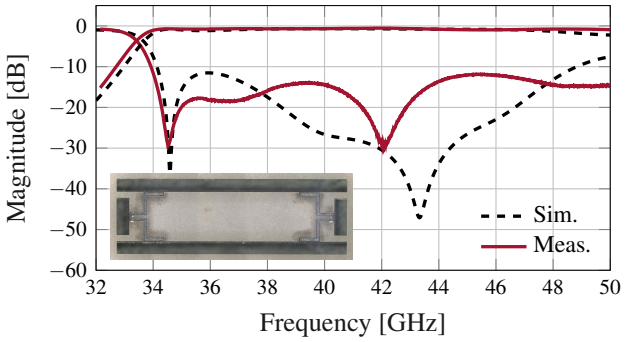

Figure 3. Rectangular waveguide S-parameters.

trenches of 350 µm were added between the waveguide and the substrate to facilitate the extraction. External excitation is performed through coplanar accesses (inset in fig. 3) engraved in the metal layer. Coplanar to waveguide transition is often the most challenging part in these kind of designs, especially on thick substrates with high electrical permittivity. Some transitions were proposed in [7] where a dipole termination with series stub is employed to adapt the line. In [8], two resonators are coupled to the access ports to excite the waveguide. This approach increases the bandwidth (BW) by sacrificing area. In order to perform the transition in the desired frequency band, coplanar accesses were optimized with 3-D EM simulation software to increase the coupling. Return loss greater than 14 dB and attenuation better than 0.13 dB/mm were measured between 39.5 GHz to 43.8 GHz for the manufactured device. Mismatches observed in the response are due to manufacturing imperfections in the coplanar accesses and differences between simulation ports and probes position.

3.3 Bandpass filters

Filters are highly demanded components in communication applications. Due to their relevance, two bandpass filter topologies aimed to operate at 40.5 - 43.5 GHz have been designed in this technology: a single-mode filter (SMF) and a single-mode filter with two transmission zeros (TZ). To accomplish return loss better than 20 dB and pass band ripple below 0.5 dB, the coupling matrix values for a 4-poles Chebyshev topology are $m_{01} = m_{45} = 1.04$, $m_{12} = m_{34} = 0.91$, $m_{23} = m_{32} = 0.7$, $m_{11} = m_{22} = m_{33} = m_{44} = 0$. Even though dual-mode filters (DM) designed in this technology [5] present good performances, the attenuation in frequencies below the bandwidth is limited due to the fundamental mode TE_{101}. Simulations performed in a 5.11 mm x 2.68 mm DM filter with the aforementioned specifications show filter rejection up to 23 dB at 34 GHz. Therefore, to enhance the rejection at low frequencies SMF were designed with TE_{101} resonators. One way to reduce the filter sensitivity is to perform inter-resonator couplings with irises placed on one side (fig. 4.a and 4.b). Despite having less coupling than a centered iris for the same length (fig. 5.a), the fluctuation linked to size dispersion is diminished, thus partially compensating the sensitivity to fabrication inaccuracy. Furthermore, this approach saves time during the

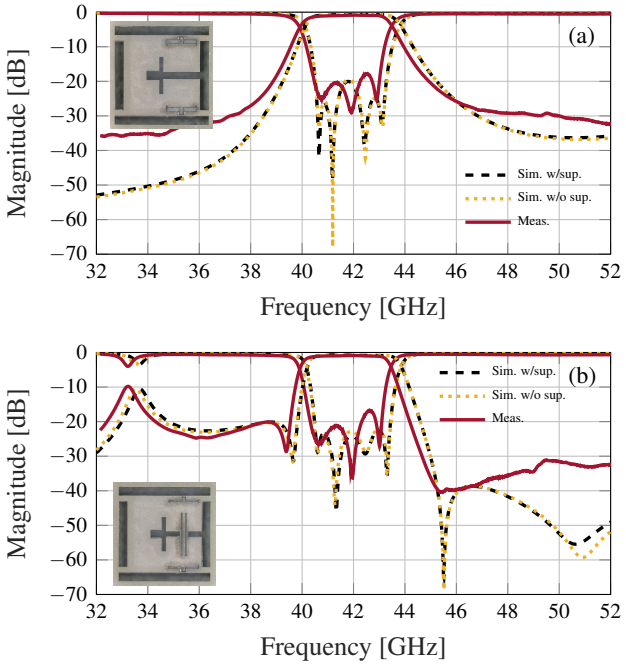

Figure 4. Measured and simulated S-parameters: single-mode filter (TE_{101}) (a) and single-mode filter w/TZ (b).

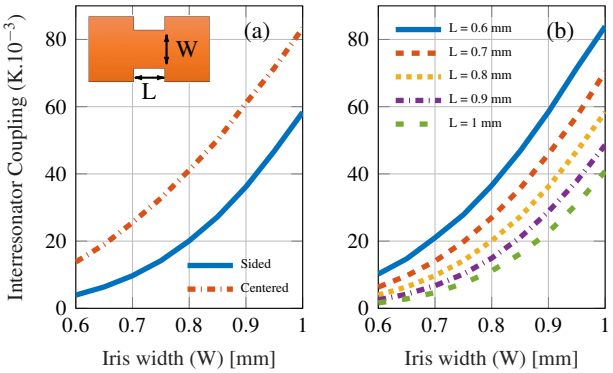

Figure 5. Inter-resonator coupling variation with: iris position ($L = 0.8mm$) (a) and length (sided) (b).

manufacturing by simplifying the pattern, leads to increasing the width for a given coupling and thus, avoids violating size restrictions that could damage the device during the cutting process. Moreover, the iris length (L) could also be modified to adjust the coupling to more convenient values (fig. 5.b). Therefore, the final design should be a good balance between mechanical robustness, sensitivity and total size. The total size for the SMF is a 3.07 mm x 3.26 mm. Measured S-parameters (Fig. 4.a) shows $RL \geq 17.7\ dB$ and $IL \leq 1.1\ dB$ at 40.35 - 43.10 GHz. In fig. 4.b, two transmission zeros have been added by means of a coplanar line between the input and the output resonators to improve the selectivity of the filter in the transition and the stop band. The target coupling matrix values are $m_{01} = m_{45} = 1.02$, $m_{12} = m_{34} = 0.87$, $m_{23} = m_{32} = 0.77$, $m_{41} = m_{14} = -0.17$, $m_{11} = m_{22} = m_{33} = m_{44} = 0$. The filter measures slightly larger than the SMF (3.13 mm x 3.24 mm). Unlike the inter-resonator couplings, the transmission line (fig. 4.b)

Table 2. Measured filters performances.

Sample		Size [mm^2]	BW [GHz]	RL [dB]	IL [dB]	Att. $_{@34GHz}$ [dB]	Att. $_{@50GHz}$ [dB]	Ripple [dB]
SMF	1	3.38 x 3.11	40.2 - 42.9	18.4	0.78	34	29	0.25
	2	3.37 x 3.11	40.4 - 43.0	17.9	0.86	35	30	0.31
	3	3.37 x 3.11	40.4 - 43.0	18.1	0.77	34	30	0.41
TZ	1	3.34 x 3.12	40.2 - 43.1	16.5	0.87	18	31	0.31
	2	3.35 x 3.12	40.2 - 43.1	14.9	0.89	18	32	0.23
	3	3.32 x 3.10	40.4 - 43.3	15.5	0.94	17	32	0.21

is centered with the resonators to have better control on the coupling with minimum influence of the iris below the line. As a result, $RL \geq 15.5\ dB$ and $IL \leq 1\ dB$ between 40.45 and 43.28 GHz are obtained. However, resonances on the line at 33.3 GHz limit the attenuation at low frequencies. In both cases, frequency shifting due to resonators sensitivity is observed. Although, manufactured devices fit properly with simulations. Three samples of each topology were fabricated to test the process repeatability with good matching in all the samples. Filter performances can be consulted in table 2 for both topologies. Supports were taken also into account during the design, and their size and position were optimized in HFSS to reduce their impact on the final response. Comparisons between filters with and without supports show negligible changes and fit with the specifications for all cases.

4 Conclusion

A characterization study of laser-machined substrate technology (LMST) has been presented. This study aims to provide fabrication constraints and design rules that helps Q-band passive-devices manufacturing. Even though it is possible to apply the process to several substrates, this work was mainly focused in low-loss Alumina substrates to improve performances. Fabrication dispersion related to laser spot uncertainty (10 µm) and imperfections on the side walls (4 - 5 µm) were identified, measured and tested in single-mode cavity resonators. The process addresses good accuracy for millimeter-wave devices manufactured in Alumina substrates up to 0.7 mm thickness. Results shows that special care must be taken during coplanar accesses engraving since external coupling sensitivity can be critical in certain devices. To reduce the sensitivity, design strategies were introduced and applied to achieve filter specifications for incoming Q-band 5G applications. Two different filter topologies were designed and manufactured showing good performances and fabrication repetability. Competitive unloadead Q around 689 at 42 GHz, better than typical SIW or LTCC processes and comparable to laser micro-machining and DRIE SOI could be obtained with proper metallization and substrate loss tangent. Even more, passive filters designed with this technology are more compact in comparison with many other technologies [5]. Finally, complex mm-Wave subsystems are expected to be developed in future work.

References

[1] M. Agiwal, A. Roy, and N. Saxena, "Next generation 5g wireless networks: A comprehensive survey," *IEEE Communications Surveys Tutorials*, vol. 18, no. 3, pp. 1617–1655, thirdquarter 2016.

[2] ITU, "ITU8 - R R15 - WRC19PREPWORK contribution 12: WRC - 19 agenda item 1.13 – IMT-2020 between 24.25 and 86 GHz," 2019. [Online]. Available: http://handle.itu.int/11.1002/doc/810730eb/81073208-en?locatt=id:1auta.

[3] W. Gautier, B. Schoenlinner, V. Ziegler, U. Prechtel, and W. Menzel, "High q micro-machined cavity resonator filter in low-cost silicon technology," in *2008 38th European Microwave Conference*, Oct 2008, pp. 1193–1196.

[4] A. Perigaud et al., "Low loss substrate integrated filters made by laser micro-machining of alumina substrates," in *2017 IEEE MTT-S International Microwave Workshop Series on Advanced Materials and Processes for RF and THz Applications (IMWS-AMP)*, Sep. 2017, pp. 1–3.

[5] A. Périgaud, K. Drissi, and N. Delhote, "Ceramic q-band bandpass filters by laser micro-machining of alumina substrates," in *2017 IEEE MTT-S International Microwave Symposium (IMS)*, June 2017, pp. 1456–1459.

[6] D. D. Marco, K. Drissi, N. Delhote, O. Tantot, P.-M. Geffroy, S. Verdeyme, and T. Chartier, "Dielectric properties of pure alumina from 8ghz to 73ghz," *Journal of the European Ceramic Society*, vol. 36, no. 14, pp. 3355 – 3361, 2016.

[7] D. Deslandes and Ke Wu, "Integrated transition of coplanar to rectangular waveguides," in *2001 IEEE MTT-S International Microwave Sympsoium Digest (Cat. No.01CH37157)*, vol. 2, May 2001, pp. 619–622 vol.2.

[8] A. Patrovsky, M. Daigle, and Ke Wu, "Millimeter-wave wideband transition from cpw to substrate integrated waveguide on electrically thick high-permittivity substrates," in *2007 European Microwave Conference*, Oct 2007, pp. 138–141.